Self-assembled periodic Fe_3O_4 nanostructures in ultrathin FeO(111) films on Ru(0001)

Guido Ketteler[1,2] and Wolfgang Ranke[1]
[1]*Department Inorganic Chemistry, Fritz-Haber-Institute of the MPG, Faradayweg 4-6, 14195 Berlin, Germany*
[2]*FU Berlin, Fachbereich Biologie, Chemie, Pharmazie, Takustr. 3, 14195 Berlin, Germany*
(Received 12 April 2002; published 17 July 2002)

Low-energy electron diffraction and scanning tunneling microscopy studies of FeO(111) films on Ru(0001) show formation of coincidence structures with a Moiré pattern up to a thickness of four monolayers. In the four monolayer thick film, strained conducting Fe_3O_4(111) nanodomains nucleate in the insulating FeO(111) matrix and form an ordered inverse biphase superstructure. Further oxidation causes these domains to grow and to coalesce into a closed Fe_3O_4(111) film.

DOI: 10.1103/PhysRevB.66.033405 PACS number(s): 68.47.Gh, 68.37.Ef, 68.65.Cd, 81.16.−c

Currently, the development of ordered metal and semiconductor nanostructures at an atomic scale with future applications as semiconducting nanodevices or quantum dot-based lasers have gained significant interest.[1,2] Arbitrary atomic scale structures are accessible by displacing atoms with the tip of a scanning tunneling microscope (STM).[3] Self-organized growth is exploited in the development of confined nanostructures.[4–6] So far, no iron oxide-based nanodevices have been developed although these would be highly interesting due to the electronic and magnetic properties of Fe_3O_4 and γ-Fe_2O_3 which are used as magnetic-field sensors and for high-density magnetic recording media.[7] Iron oxides are also of high importance for a number of catalytic reactions,[8] in particular the dehydrogenation of ethylbenzene to styrene.[9,10] Well-defined oxide films grown on metal substrates have gained interest as model catalysts since the conducting substrate allows one to apply surface science techniques using charged particles. Ultrathin films are also of interest with respect to phase transitions as the high surface to bulk ratio may change the transition behavior as known for the surface melting of metals and semiconductors[11] or the premelting of ice.[12] Growth of ultrathin FeO(111) films on Pt(111) revealed that the growth of ionic films is quite different when compared to covalent compounds in that minimization of the Madelung energy is of higher importance for the structure of such films than strain.[13] In order to investigate whether this behavior can be generalized, we investigated the growth of iron oxides on Ru(0001). Fe films on this substrate are also of interest due to issues surrounding ultrathin film magnetism[14,15] and as bimetallic catalysts for the ammonia and Fischer–Tropsch synthesis.[16,17]

The experiments were performed in an ultrahigh vacuum chamber with a base pressure of 1×10^{-10} mbar.[18] It is equipped with a scanning tunnelling microscope (Burleigh), combined low-energy electron diffraction (LEED), and Auger electron spectroscopy (AES) optics, a sputter gun, and gas inlet valves for O_2 and Ar. Iron was evaporated by resistively heating an iron wire wrapped around a tungsten filament. FeO(111) films were prepared by deposition of iron onto a clean Ru(0001) substrate and subsequent oxidation in 10^{-6} mbar O_2, initially at 870 K and finally at 1000 K. Large-scale STM images, AES intensity ratios of Ru (273 eV), Fe (651 eV), O (503 eV), and observation of the vanishing of the O/Ru(0001)-(2×2) LEED pattern were used to obtain an estimate of coverages. The exact thickness is uncertain since some iron diffuses into the Ru substrate, depending on annealing time, temperature and O_2 pressure. Exposure of the clean Ru(0001) to 10^{-6} mbar O_2 for up to 1 h results only in the formation of the O/Ru(0001)-(2×2) structure and no ruthenium oxides are formed which require stronger oxidizing conditions.[19]

FeO(111) films grown on Ru(0001) display characteristic LEED patterns which can be regarded as a Ru(0001)-(8×8) pattern [Fig. 1(a)]. A schematic view of one FeO(111) bilayer on Ru(0001) is shown in Fig. 1(b). The hexagonally arranged spots marked by an arrow in Fig. 1(a) correspond to Ru(0001)-(1×1) spots. This pattern is superimposed on the hexagonal first-order FeO spots located closer to the specular beam. The unit cell of the FeO(111) film is slightly expanded and can be estimated from the LEED pattern to be ~3.08 Å (bulk, 3.04 Å). FeO(10) spots are surrounded by hexagonally arranged satellite spots. With increasing coverage, the FeO(10) spot intensity increases while the satellite spots get weaker. This suggests that they result mainly from multiple scattering between the FeO(111) film and the Ru(0001) substrate rather than from diffraction at the large Moiré unit cell visible in the STM images (see Fig. 2). Similar LEED patterns were observed for ultrathin FeO(111) films on Pt(111).[13,20] There, four different Moiré superstructures representing different coincidence structures with the Pt(111) substrate were observed, depending on the FeO(111) coverage up to 2.5 ML. Only beyond 2 ML FeO(111) coverage, unrotated (8×8) LEED patterns were obtained on Pt(111). The LEED patterns from FeO(111) films with thicknesses between 0–4 ML on Ru(0001) are much sharper than those on Pt(111) and no elongations or spot splittings occur indicating that the superstructures are not rotated, very well or-

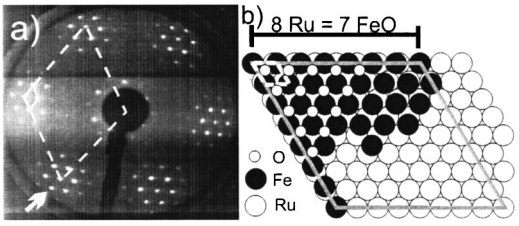

FIG. 1. One monolayer FeO(111) on Ru(0001): (a) LEED image (60 eV); (b) schematic top view.

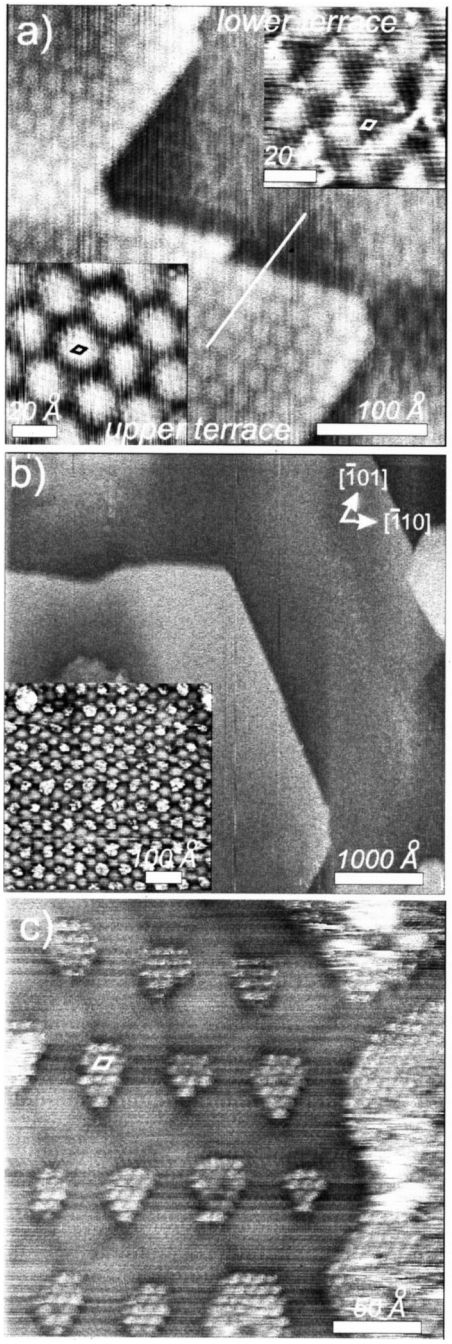

FIG. 2. (a) 400×400 Å^2 ($I_t=0.2$ nA, $U_B=+0.45$ V) STM images of ~2.1 ML FeO(111)/Ru(0001). A second (right) and third (left) FeO(111) monolayer terrace with their Moiré patterns are separated by a zig–zag shaped step. The insets show 70×70 Å^2 (right, $I_t=0.2$ nA, $U_B=+0.45$ V) and 80×80 Å^2 (left, $I_t=0.2$ nA, $U_B=+0.7$ V) STM images of the second and third FeO(111) monolayer, respectively. The diamonds indicate the respective unit cells of the protrusions on both terraces with unit cell vectors of 3.1 Å (right) and 3.55 Å (left). The white line shows the alignment of the Moiré pattern on both domains. (b) 5000×5000 Å^2 ($I_t=0.3$ nA, $U_B=+1.0$ V) STM image of ~4 ML thick FeO(111)/Ru(0001). The inset shows a 600×600 Å^2 region of one terrace ($I_t=0.4$ nA, $U_B=+0.7$ V). (c) 250×250 Å^2 ($I_t=0.3$ nA, $U_B=+0.7$ V) STM image showing self-ordered $Fe_3O_4(111)$ domains embedded in the FeO(111) film.

dered and highly oriented with respect to the Ru(0001) substrate. The (8×8)-superstructure periodicity is 21.6 Å and results from the coincidence of 7 FeO units with 8 Ru atoms.

Figure 2 shows STM images of FeO(111) films of various thickness. All atomic steps in the FeO(111) films are perfectly aligned with the Moiré pattern. We attribute the FeO(111) superstructure on the lower terrace in Fig. 2(a) (right side) to second layer FeO(111). It covers nearly the whole film. The superstructure on the upper terrace [left side of Fig. 2(a)] corresponds to the third layer FeO(111). Higher resolution images shown as insets in Fig. 2(a) resolve different types of Moiré patterns. The bright round regions and the atomic features with a periodicity of ~3.55 Å on the upper terrace correspond to strongly expanded FeO with 6 FeO units on 8 Ru atoms. On the lower terrace, the bright regions are triangular with an atomic periodicity of ~3.1 Å. In both cases the Moiré periodicity is ~21.5 Å and fits with the value estimated from the LEED pattern. On the lower terrace, bright triangular lines are resolved which connect 2–6 Moiré features and are one atomic feature wide.

A thicker film is shown in Figs. 2(b) and 2(c). According to the deposited amount of iron and the intensity of the Fe peak in AES, it is 4 ML thick and has a new superstructure. The film is very flat with terrace widths of ~1500 Å [Fig. 2(b)]. Closer inspection reveals bright islandlike domains forming a distorted hexagonal pattern with unit cell vectors of ~50 and ~65 Å [Fig. 2(c) and inset in Fig. 2(b)] embedded in an FeO(111) Moiré structure. We interpret them as $Fe_3O_4(111)$ domains since very similar tunneling conditions are necessary to image atomic features as on $Fe_3O_4(111)$ films on Ru(0001) (see below) and on Pt(111),[21] whereas different tunneling conditions are favorable for FeO(111) regions. The different chemical nature becomes evident after several hours of tunneling when the bright domains become adsorbate covered while the rest remains adsorbate-free in agreement with observations for FeO(111) and $Fe_3O_4(111)$ films on Pt(111).[22] High tunneling currents can be obtained on the bright domains suggesting a high conductivity. The periodicity within them is ~7 Å. On bulk $Fe_3O_4(111)$, the periodicity is ~6 Å and corresponds to $\frac{1}{4}$ ML of iron atoms on top of a hexagonal oxygen layer.[21] The O–O distance on the bright domains has thus the same expanded value of 3.5 Å as the FeO(111) layer from which it emerged. Generally, the protrusions from different domains are not in registry. Also more extended domains can be seen [right-hand side of Fig. 2(c)] as well as regions where no such domains have formed. In analogy to the "biphase ordering" [23,24] of triangular FeO(111) domains on $Fe_3O_4(111)$ or α-$Fe_2O_3(0001)$, we call the formation of ordered $Fe_3O_4(111)$ domains in a FeO(111) substrate "inverse biphase ordering." However, the origin and stabilization of this superstructure is not the mismatch between one iron oxide phase situated on top of another as will be discussed below and thus is quite different compared to the biphase ordered structures found by Condon *et al.*

Upon further oxidation for 20 min, the satellite LEED pattern of the FeO(111) film vanishes and the normal $Fe_3O_4(111)$ pattern with the unexpanded lattice constant of ~6 Å (Ref. 21) appears [Fig. 3(a)]. The STM images [Fig.

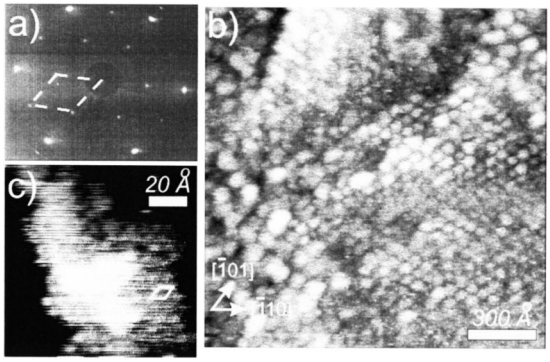

FIG. 3. (a) LEED pattern (60 eV) of the film shown in Figs. 2(b) and 2(c) after further oxidation. (b) 1500×1500 Å^2 ($I_t=1.0$ nA, $U_B=-0.2$ V) STM image. (c) 100×100 Å^2 ($I_t=0.3$ nA, $U_B=+0.9$ V) section of one terrace. The diamond indicates the unit cell of the protrusions with an unit cell vector of 6 Å.

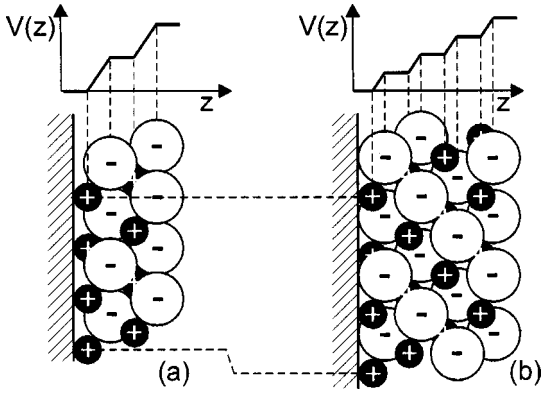

FIG. 4. Layer structure of FeO(111) on Ru and dipole induced surface potential. (a) For 2 ML, slightly relaxed FeO structure (O–O distance 3.10 Å). (b) For 4 ML, strongly relaxed (O–O distance 3.58 Å).

3(b)] show clusterlike features with diameters between 30 and 100 Å with the same $\sim6\times6$ Å periodicity [Fig. 3(c)]. In some regions, the clusters form a pseudohexagonal arrangement with a unit cell of $\sim53(\pm9)$ by $\sim62(\pm9)$ Å which fits the periodicity of the $Fe_3O_4(111)$ domains in Fig. 2(c). This indicates that the superstructure of expanded $Fe_3O_4(111)$ domains on FeO(111) represents the nucleation stage of the thermodynamically favored phase transition[25] to $Fe_3O_4(111)$. The change in stoichiometry to a more oxygen-rich phase is also reflected in a decrease of the Fe/O Auger intensity ratio from about 0.36 to 0.24.

On Pt(111), FeO(111) grows layer-by-layer (Frank–Van der Merwe growth mode) up to a thickness of ~2.5 ML before growth of statistically arranged $Fe_3O_4(111)$ islands starts, resulting in an overall Stranski–Krastanov growth mode.[26] Upon repeated cycles of deposition of very small Fe amounts and subsequent oxidation (i.e., closer to thermodynamic equilibrium), the same growth mode was found on Ru(0001) while the metastable structures shown in Fig. 2 were only obtained after deposition of the corresponding amount of Fe in one turn. On both metals, growth is not pseudomorphic and specific coincidence structures with the substrate are formed. For the surface free energies of FeO and Ru values of 0.6 J/m^2 (Ref. 27) and 2.93 J/m^2 (Ref. 28) have been reported. These values support the observed wetting behavior and growth mode.

FeO(111) films on Pt(111) are oxygen terminated and bound via an iron layer to the substrate.[29,30] Since the Ru(0001) substrate does not react to form ruthenium oxide, and the chemisorbed O/Ru(0001)-(2×2) phase can easily be replaced by the FeO(111) film, and since LEED patterns and STM images look quite similar on Pt(111) and Ru(0001), we expect the same stacking sequence on Ru(0001). According to the concept introduced by Tasker,[31,32] the stability of such polar films decreases with thickness z since each iron–oxygen bilayer produces an electrostatic field $E=\sigma/\varepsilon_0$ (σ = charge density within the planes) which increases the surface potential $V(z)$ of the film. This results in a thickness-dependent electrostatic surface energy $\gamma_{f,n}$ which increases with the number of layers n as shown schematically in Fig. 4. FeO(111) bilayers can only be stabilized up to a certain thickness $n_{\max}$ and large relaxations and charge redistributions are required to reduce the electrostatic surface energy.[13] This critical thickness seems to be ~4 ML on Ru(0001). FeO(111) films of this thickness could not be obtained on Pt(111).

Periodic self-assembled nanostructures on metal or semiconductor surfaces are often obtained by growth on periodic strain-relief patterns.[5,6] In ionic films, the bonds are not strongly directed. In order to reduce the Fe–O layer dipoles and thus the Madelung energy, the Fe–O layer distances within the bilayers perpendicular to the surface may decrease. In order to keep the atomic distances, the lattice is expanded parallel to the surface. Figure 4(a) shows the situation for a FeO film with the only slightly expanded O–O distance of 3.10 Å parallel to the surface (bulk value 3.04 Å) as observed up to 2 ML. All layer distances are approximately equal. When the third and fourth ML are formed [Fig. 4(b)], the lattice was found to expand (O–O distance 3.58 Å) and within each bilayer the layer distance is reduced from 1.25 Å (bulk value) to about 0.6 Å when assuming constant Fe–O bond distances. The dipole potential per bilayer is reduced correspondingly. The layer distance between the bilayers is assumed almost unchanged, otherwise the ionic spheres of oxygen would overlap. Nevertheless, as the bonds in oxides are not purely ionic, already slight changes of the covalent vs ionic character may enable a significant gain in the Madelung energy. For example, if the Fe–O bond length within the bilayer would decrease as observed for the first FeO layer on Pt(111),[13] relaxation and layered character might be even more pronounced.

Also the formation of $Fe_3O_4(111)$ domains reduces the average Madelung energy since $Fe_3O_4(111)$ is terminated by $\frac{1}{4}$ ML of Fe.[21] One reason why a $Fe_3O_4(111)$ film, although thermodynamically favorable,[25] cannot be formed from the beginning, is its large unit cell. In the [111] direction, equivalent repeat units are 4.85 Å high consisting of two O and two inequivalent Fe-sublayers each. More than one repeat unit seems necessary to stabilize the structure. Compared to FeO, the occupation of the Fe-sublayers in Fe_3O_4 is only $\frac{3}{4}$. Keeping the Fe amount constant, exactly five Fe-layers in Fe_3O_4 plus $\frac{1}{4}$ layer as surface termination can be produced from

four full Fe layers in FeO under oxidative conditions. The minimum FeO film thickness for such a stoichiometric conversion is 4 ML, where we in fact have observed it. Initially, the Fe_3O_4 domains keep the in-plane lattice expansion of the FeO film and do not change it to the bulk value before oxidation of the whole film. The $Fe_3O_4(111)$ domains form at crossing points of dark lines in the FeO(111) Moiré pattern [Figs. 2(b) and 2(c)]. For FeO films on Pt(111), dark areas correspond to topographically higher regions.[30] If this applies to Ru, too, these are areas where the destabilizing polar oxygen termination rises up representing locally the most instable regions. Nucleation of Fe_3O_4 on these positions reduces the Madelung energy most effectively. Also concerning interface energetics, these sites may be unfavorable since the first layer iron atoms are forced to occupy on-top sites of the substrate.

In summary, well ordered FeO(111) films can be grown on Ru(0001) up to larger thicknesses than on Pt(111). Depending on thickness, they relax and form different Moiré patterns with their atomic rows aligned to those of the substrate. When 4 ML are reached, strained Fe_3O_4 domains nucleate at particular sites of the FeO(111) Moiré pattern so that a self-assembled regular arrangement of $Fe_3O_4(111)$ nanodomains is formed in the FeO(111) matrix. No additional Fe is needed for this transition. The driving forces are thermodynamics and the reduction of the surface Madelung energy rather than strain effects. The nanodomains are metastable and larger Fe_3O_4 clusters and finally a closed film forms after prolonged oxidation at high temperature. The nanostructures may open interesting applications as nanodevices since both oxides have strongly different electronic and magnetic properties. FeO(111) is insulating and unmagnetic while $Fe_3O_4(111)$ has metallic conductivity and is ferrimagnetic. An investigation of the magnetic properties of these nanostructures with spin-polarized STM as has been performed for $Fe_3O_4(001)$ surfaces[33] appears promising.

We thank Thomas Bunke and Robert Schlögl for discussions and support.

[1] A. O. Orlov, I. Amlani, G. H. Bernstein, C. S. Lent, and G. L. Snider, Science **277**, 928 (1997).
[2] N. N. Ledentsov, V. M. Ustinov, V. A. Shchukin, P. S. Kopev, Z. I. Alferov, and D. Bimberg, Semiconductors **32**, 343 (1998).
[3] D. M. Eigler and E. K. Schweizer, Nature (London) **344**, 524 (1990).
[4] R. Nötzel, J. Tommyo, and T. Tamamura, Nature (London) **369**, 131 (1994).
[5] H. Brune, M. Giovannini, K. Bromann, and K. Kern, Nature (London) **394**, 451 (1998).
[6] H. Brune, Surf. Sci. Rep. **31**, 125 (1998).
[7] J. C. Mallison, *The Foundations of Magnetic Recording*, 2nd ed. (Academic, New York, 1993).
[8] J. W. Geus, Appl. Catal. **25**, 313 (1986).
[9] M. Muhler, R. Schlögl, and G. Ertl, J. Catal. **138**, 413 (1992).
[10] C. Kuhrs, Y. Arita, W. Weiss, W. Ranke, and R. Schlögl, Top. Catal. **14**, 111 (2001).
[11] L. Wojtczak and J. H. Rutkowski, Prog. Surf. Sci. **59**, 79 (1998).
[12] J. G. Dash, H. Fu, and J. S. Wettlaufer, Rep. Prog. Phys. **58**, 115 (1995).
[13] W. Ranke, M. Ritter, and W. Weiss, Phys. Rev. B **60**, 1527 (1999).
[14] J. P. Sanchez, M. F. Ravet, M. Piecuch, and M. Maurer, Hyperfine Interact. **57**, 2077 (1990).
[15] C. Liu and S. D. Bader, Phys. Rev. B **41**, 553 (1990).
[16] F. J. Berry, L. Liwu, W. Chengyu, T. Renyuan, Z. Su, and L. Dongbai, J. Chem. Soc., Faraday Trans. 1 **81**, 2293 (1985).
[17] K. Urabe and A. Ozaki, J. Catal. **52**, 542 (1978).
[18] W. Weiss, M. Ritter, D. Zscherpel, M. Swoboda, and R. Schlögl, J. Vac. Sci. Technol. A **16**, 21 (1998).
[19] Y. D. Kim, A. P. Seitsonen, S. Wendt, J. Wang, C. Fan, K. Jacobi, H. Over, and G. Ertl, J. Phys. Chem. B **105**, 3752 (2001).
[20] M. Ritter, W. Ranke, and W. Weiss, Phys. Rev. B **57**, 7240 (1998).
[21] M. Ritter and W. Weiss, Surf. Sci. **432**, 81 (1999).
[22] Sh. Shaikhutdinov and W. Weiss, J. Mol. Catal. A: Chem. **158**, 129 (2000).
[23] N. G. Condon, F. M. Leibsle, T. Parker, A. R. Lennie, D. J. Vaughan, and G. Thornton, Phys. Rev. B **55**, 15 885 (1997).
[24] N. G. Condon, F. M. Leibsle, A. R. Lennie, P. W. Murray, D. J. Vaughan, and G. Thornton, Phys. Rev. Lett. **75**, 1961 (1995).
[25] G. Ketteler, W. Weiss, W. Ranke, and R. Schlögl, Phys. Chem. Chem. Phys. **3**, 1114 (2001).
[26] W. Weiss and M. Ritter, Phys. Rev. B **59**, 5201 (1999).
[27] S. H. Overbury, P. A. Bertrand, and G. A. Somorjai, Chem. Rev. **75**, 547 (1975).
[28] H. A. Gasteiger, P. N. Ross, and E. J. Cairns, Surf. Sci. **293**, 67 (1993).
[29] C. S. Fadley, M. A. Van Hove, Z. Hussain, and A. P. Kaduwela, J. Electron Spectrosc. Relat. Phenom. **75**, 273 (1995).
[30] H. C. Galloway, P. Sautet, and M. Salmeron, Phys. Rev. B **54**, R11 145 (1996).
[31] P. W. Tasker, J. Phys. C **12**, 4977 (1979).
[32] C. Noguera, J. Phys.: Condens. Matter **12**, R367 (2000).
[33] R. Wiesendanger, I. V. Shvets, D. Bürgler, G. Tarrach, H.-J. Güntherodt, J. M. D. Coey, and S. Gräser, Science **255**, 583 (1992).